Journal of Earthquake Engineering

ISSN: (Print) (Online) Journal homepage: https://www.tandfonline.com/loi/ueqe20

Ground Motion Correlations from Recorded Mexican Intermediate-depth, Intraslab Earthquakes

Miguel A. Jaimes, Gabriel Candia, Alhelí S. López-Castañeda & Jorge Macedo

To cite this article: Miguel A. Jaimes, Gabriel Candia, Alhelí S. López-Castañeda & Jorge Macedo (2021): Ground Motion Correlations from Recorded Mexican Intermediate-depth, Intraslab Earthquakes, Journal of Earthquake Engineering, DOI: 10.1080/13632469.2021.2001393

To link to this article: https://doi.org/10.1080/13632469.2021.2001393

Published online: 06 Dec 2021.

JOURNAL OF EARTHQUAKE ENGINEERING
https://doi.org/10.1080/13632469.2021.2001393

Taylor & Francis
Taylor & Francis Group

Ground Motion Correlations from Recorded Mexican Intermediate-depth, Intraslab Earthquakes

Miguel A. Jaimes[a], Gabriel Candia[b], Alhelí S. López-Castañeda[a], and Jorge Macedo[c]

[a]Coordinación de Ingeniería Estructural, Instituto de Ingeniería, UNAM, Ciudad de México, México; [b]Facultad de Ingeniería Civil, Universidad del Desarrollo, and National Research Center for Integrated Natural Disaster Management (CIGIDEN), Santiago, Chile; [c]Geosystems Engineering, Georgia Institute of Technology, Atlanta, Georgia, USA

ABSTRACT

Predictive models to estimate correlation coefficients between peak ground acceleration, peak ground velocity, and spectral acceleration residuals for Mexican intermediate-depth, intraslab earthquakes recorded on rock sites are presented in this study. The models were developed for the total, between-events, and within-event residuals using a recent ground-motion prediction equation (GMPE) and an updated ground-motion database. The results support the use of region- and mechanism-specific correlation models for the subduction intraslab zone of Mexico. An example of the application of the proposed correlation coefficient models consisting in evaluating a conditional mean spectrum (CMS), based on the Mexican seismic design normative, is presented.

ARTICLE HISTORY
Received 8 June 2020
Accepted 29 October 2021

KEYWORDS
Intermediate-depth; intraslab earthquakes; ground-motion intensity measures; linear correlation coefficient; conditional mean spectrum

1. Introduction

Single ground-motion intensity measures (IMs), such as peak ground acceleration (PGA) or pseudo spectral acceleration values (Sa), are often used as proxies for the seismic response of structural and geotechnical systems. However, in many practical applications, the seismic response of a system is better described in terms of two or more jointly occurring ground-motion IMs, which requires the knowledge of the correlation coefficient between such IMs. Extensive research has been conducted to quantify the statistical dependence between IMs. Particularly, several studies have developed empirical models for the linear correlation between Sa pairs based on the Pearson's correlation coefficient (PCC) (Azarbakht et al. 2014; Baker and Cornell 2006; Baker and Jayaram 2008; Bradley 2011; Jayaram et al. 2011). Baker and Cornell (2006) used a global database of shallow-crustal earthquakes to develop Sa correlations from a single ground-motion component as well as Sa correlations from two orthogonal components at two differing periods. From the results, the authors observed that the correlation values were insensitive to the underlying GMPE, and practically independent of magnitude or distance. Based on the work of Baker and Cornell (2006), Baker and Jayaram (2008) presented correlation models for several definitions of spectral acceleration at two periods in the 0.01 s to 10 s range. Specifically, they used the NGA ground-motion database (Chiou et al. 2008) for shallow-crustal earthquakes, and four GMPEs from the NGA project. Their results were in good agreement with previous studies. Later, Jayaram et al. (2011) computed Sa correlations using a ground-motion dataset from subduction and shallow-crustal earthquakes recorded in Japan. They evaluated the effects of the GMPE, source mechanism, style of faulting, seismic zone, site conditions, and site-to-source distance on the estimated correlations. The authors found systematic differences between correlation coefficients within three ground-motion subsets (i.e., active crustal zone, subduction interface zone, and subduction slab zone). They attributed such differences to the energy content associated to each

CONTACT Miguel A. Jaimes mjaimest@iingen.unam.mx Instituto de Ingeniería, UNAM, Coordinación de Ingeniería Estructural, Edificio 2, Piso 3, Cub. 305, Circuito Escolar Universitario, Ciudad de México 04510, México

tectonic environment. Regarding the style of faulting, the correlation analyses revealed that the differences were in part due to the limited number of ground motions within each category (i.e., records from normal, oblique, reverse, and strike-slip faulting). The authors concluded that earthquake magnitude and source-to-site distance have negligible effects on Sa correlations. More recently, Daneshvar, Bouaanani, and Godia (2015) presented an inter-period correlation model over the range 0.01 s to 5 s, using 108 horizontal accelerograms from 8 earthquakes recorded in Eastern Canada, which is a region with moderate seismic activity. They showed that inter-period correlations were more sensitive to magnitude than distance. Furthermore, the authors revealed that the correlation coefficients for Eastern Canada were higher than Baker and Jayaram (2008) predictions for shallow-crustal earthquakes. Kotha, Bindi, and Cotton (2017) developed correlation models for Europe and Middle Eastern regions using ~6000 ground motions from the RESORCE database and the GMPE by Bindi et al. (2014) for a period range between 0.02 s and 4 s. They observed significant magnitude dependence associated with the between-events residuals, and that near-source events and site corrected residual correlations are region-dependent. In the case of Mexico, Jaimes and Candia (2019) presented Sa correlation coefficients using subduction interface ground motions recorded on rock sites. They reported significative differences with respect to previous global and regional studies.

Other studies have derived correlation coefficients without providing explicit models. For example, Inoue and Cornell (1990) studied the correlation between IMs derived from a single ground motion component. Also, several authors have studied correlations between IMs different from Sa. For instance, Trombetti et al. (2008) presented correlation coefficients between PGA, peak ground velocity (PGV), and peak ground displacement (PGD) values. The analysis was based on 344 accelerograms recorded on soil NEHRP Class C; the number of recorded events earthquake and their source mechanisms were not reported. The authors reported positive values between 0.65 and 0.70 for both PGA-PGV and PGV-PGD correlations, whereas a weak correlation for PGA-PGD.

The aforementioned models are widely used in earthquake engineering applications, such as: (a) vector-valued (or multivariate) probabilistic seismic hazard analysis (Bazzurro and Cornell 2002; Goda and Atkinson 2009); (b) the construction of conditional spectra (Baker 2011; Carlton and Abrahamson 2014; Daneshvar, Bouaanani, and Godia 2015; Lin et al. 2013); (c) the simulation of response spectra given an earthquake scenario (Baker and Cornell 2006); and (d) seismic risk assessment of interdependent infrastructure (Cordova et al. 2001; Inoue and Cornell 1990).

With a few exceptions, most region-specific correlation models have been developed for shallow-crustal earthquake zones. The existing literature on ground-motion correlations from subduction earthquakes is still limited. For instance, southern Mexico is a diverse tectonic setting exposed to ground motions from both interface and intraslab earthquakes, and to significantly less frequent shallow-crustal earthquakes occurring in the Trans-Mexican Volcanic Belt. However, the applicability of global or regional models from outside Mexico to the local intraslab tectonic setting in Mexico has not been studied. This article provides empirical correlations between PGA, PGV, and Sa using strong-motion recordings from Mexican intermediate-depth, intraslab earthquakes. Then, the empirical coefficients are used to build a continuous closed-form correlation model. Finally, the results are compared to existing models worldwide, and its use is illustrated through a CMS calculation for a site located in south-central Mexico.

1.1. Assessment of Correlation between Two Ground-motion Intensity Measures

Ground-motion IMs at a site are commonly obtained from GMPEs, which are developed via semi-empirical regressions on selected strong motion data. A GMPE usually has the form

$$Y = f(X_k) + \varepsilon\sigma \tag{1}$$

where Y, the natural logarithm of I, is described as a normal random variable with mean $f(X_k)$ and total standard deviation σ. The mean is a function of explanatory variables X_k that usually include the earthquake magnitude (M), a measure of the source-to-site distance (R), and other variables (θ) that

may include the style of faulting and site-specific parameters, among other factors. The term ε, known as *normalized residual*, is a standard normal random variable that represents the variability of Y. By rearranging Equation 1, ε can be interpreted as the number of standard deviations between the observation and the mean of the ground-motion IM, thus

$$\varepsilon = \frac{Y - f(X_k)}{\sigma} \tag{2}$$

The product between the normalized residual and the total standard deviation, i.e., $\varepsilon\sigma$ in Equation 1, stands for the ground-motion residual, hereafter denoted δ. It is customary to split δ into a between-events residual (δ_B) and a within-event residual (δ_W), which are independent normal random variables with zero-mean and standard deviations σ_B and σ_W, respectively. The standard deviation σ_B, known as *inter-event variability*, stands for the combined ground-motion variability resulting from event specific factors that have not been included in the predictive model, whereas σ_W, known as *intra-event variability*, stands for the combined ground-motion variability coming from record-specific factors. Since between-events and within-event residuals are independent random variables, the total standard deviation of the ground-motion model can be computed as

$$\sigma = \sqrt{\sigma_B^2 + \sigma_W^2} \tag{3}$$

and the total residual as

$$\delta = \varepsilon\ \sigma = \varepsilon_B\sigma_B + \varepsilon_W\sigma_W \tag{4}$$

where ε_B and ε_W are the normalized between-events and within-event residuals, respectively.

From the linear relationship between Y and ε observed in Equation 1, the correlation between any pair of ground-motion IMs, say IM_1 and IM_2, is equal to the correlation between their correspondent normalized residuals, ε_1 and ε_2, respectively. PCC is chosen to measure the statistical dependence between these IMs. Thus, in a database of n ground motions the linear correlation between ε_1 and ε_2 is given by

$$\rho_{\varepsilon_1,\varepsilon_2} = \frac{\sum_{i=1}^{n}(\varepsilon_{1i} - \overline{\varepsilon_1})(\varepsilon_{2i} - \overline{\varepsilon_2})}{\sqrt{\sum_{i=1}^{n}(\varepsilon_{1i} - \overline{\varepsilon_1})^2 \sum_{i=1}^{n}(\varepsilon_{2i} - \overline{\varepsilon_2})^2}} \tag{5}$$

where ε_{1i} is the IM_1 residual in the i-th ground motion, $\overline{\varepsilon_1} = \frac{1}{n}\sum_{i=1}^{n}\varepsilon_{1i}$ is the sample mean for ε_1. Analogous definitions apply for ε_{2i} and $\overline{\varepsilon_2}$. If the partition of the residuals is considered as in Equation 4, the total correlation can be written as:

$$\rho_{\varepsilon_1,\varepsilon_2} = \frac{\sigma_{B1}\sigma_{B2}\rho_B + \sigma_{W1}\sigma_{W2}\rho_W}{\sigma_1\sigma_2} \tag{6}$$

where σ_{Bk}, σ_{Wk}, and σ_k are the between-events, within-event, and total standard deviations of IM_k, $k = 1, 2$, respectively. Here, ρ_B and ρ_W s tand for the correlation coefficients of the normalized between-events and within-event residuals, respectively, which can be estimated individually using Equation 5. A flowchart of the methodology is presented in Fig. 1.

2. Data and Estimation of Correlation Coefficients

2.1. Intensity Measures Examined

Correlation coefficients were computed for the quadratic mean of the two horizontal orthogonal components of: (1) peak ground acceleration (*PGA*), (2) peak ground velocity (*PGV*), and (3) pseudo-acceleration response spectra (*Sa*), 5% damped, for periods between 0.01 s and 5 s.

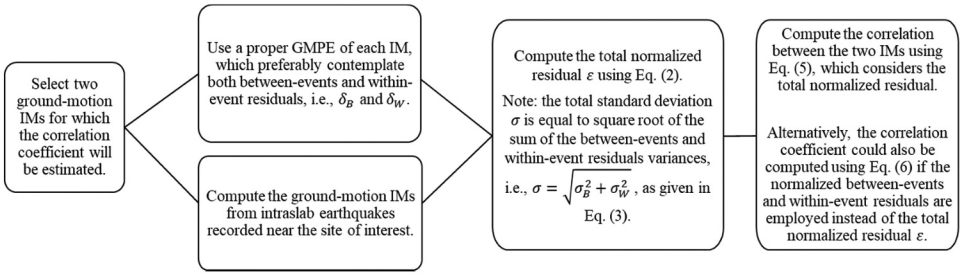

Figure 1. Flowchart of the methodology employed for the computation of the correlation coefficient for two ground-motion IMs.

2.2. Strong-motion Dataset

Observed *PGA*, *PGV*, and *Sa* values were obtained from the RAII-UNAM strong motion database (II-UNAM 2020) and based on the work by García (2006) and Jaimes and García-Soto (2020). The selected dataset includes 366 two-component records from 23 intermediate-depth, intraslab earthquakes, recorded at 69 stations located on rock site. The subset includes earthquakes with moment magnitudes between 5 and 8.2, rupture distances between 54 km and 400 km, and focal depths from 35 km to 138 km. It should be noted that sites that present site effects have been excluded from the database used in this study. Such sites were selected based on a rigorous exploration of the data and following the works by García (2006) and Jaimes and García-Soto (2020). As all sites considered in the database exhibit almost constant behaviour, there is expected an unsignificant change in, for example, their natural vibration periods. Thus, any variation in the dominant period of the soil will not considerably affect the computed correlations.

A summary of the ground-motion parameters is presented in Table A1. Figure 2 shows a map of Central Mexico showing the geographical localization of the earthquakes and recording stations considered in this study. Figure 3 shows the distribution of moment magnitude and focal depth data in distance, respectively. All accelerograms were processed using a high-pass filter with corner frequency of 0.05 Hz for events with $M_w >$ 6.5, and 0.1 Hz for the remaining events.

2.3. Ground-motion Prediction Equations

The current study uses the GMPEs developed by Jaimes and García-Soto (2020) for intermediate-depth, intraslab earthquakes. These GMPEs were derived using a mixed-effects model for the quadratic mean of the horizontal components of *PGA*, *PGV*, and 5% damped *Sa* for periods between 0.01 s and 5 s. The proposed functional form for $Y = \ln(SaorPGAorPGV)$ is

$$Y = \alpha_1 + \alpha_2 M_w + \alpha_3 \ln(R) + \alpha_4 R + \alpha_5 H \tag{7}$$

where $R = \sqrt{D^2 + \Delta^2}$, D (in km) is the closest distance from site to the rupture plane for events with $M_w >$ 6.5, or the hypocentral distance for events with $M_w \leq$ 6.5; $\Delta = 0.0075 \cdot 10^{0.507 M_w}$ (in km) is a near-source saturation term; $H = (\min(H_D, 75) - 50)$ (in km) is the depth scaling term, and H_D (in km) is the focal depth of the event. The regression coefficients α_1 to α_5 and standard deviations are summarized in Table A2 for *Sa*, *PGA*, and *PGV* in units of cm/s^2, cm/s^2, and cm/s, respectively. The period dependence of the total, within-event, and between-events standard deviations is shown in Fig. 4; from this figure is apparent that the total standard deviation is controlled by the intra-event variability.

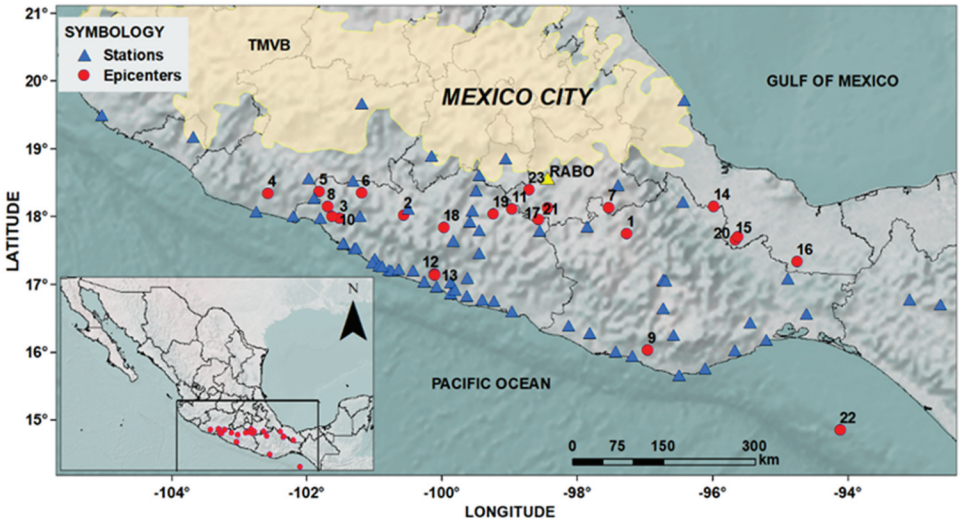

Figure 2. Map of Central Mexico showing epicenters (circles) of intermediate-depth, intraslab earthquakes and recording stations (triangles) considered in this study. The shaded area corresponds to the Trans-Mexican Volcanic Belt (TMVB).

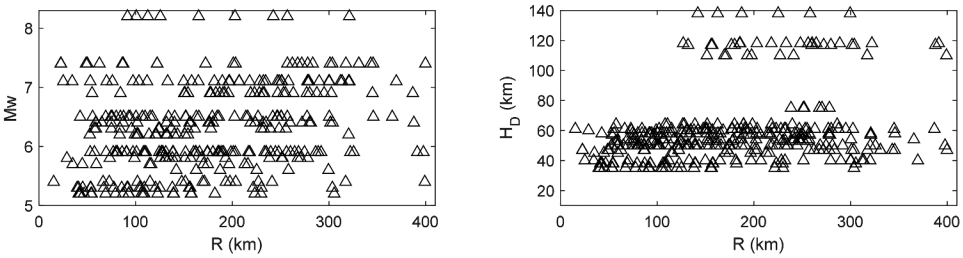

Figure 3. Distribution of magnitude and focal depth data in distance.

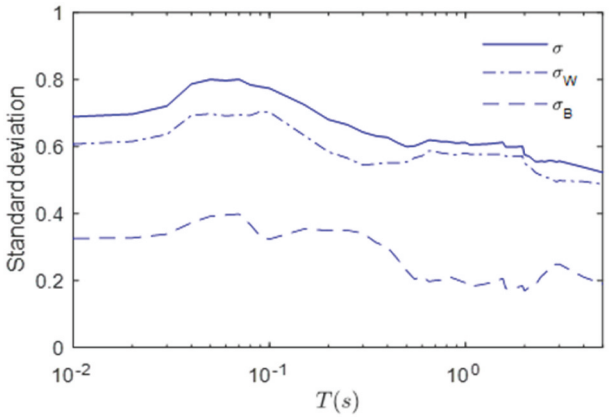

Figure 4. Estimated standard deviations of total residuals σ, between-events residuals σ_B, and within-event residuals σ_W for $Sa(T)$ considering the GMPEs developed by Jaimes and García-Soto (2020).

2.4. Correlation Coefficient Calculations

Using the RAII-UNAM strong-motion dataset and the GMPEs by Jaimes and García-Soto (2020), the correlation for total residuals was computed for different ground-motion IMs. The results are summarized in Table A3 and in Fig. 5 as contour plots. In addition, correlation coefficients for between-events and within-event residuals are presented in Table A4 and Table A5, respectively. From Fig. 5 it is verified that the total and within-event correlations are very similar for all IM pairs analysed.

A standard nonlinear least-squares regression of the total correlation coefficients presented in Table A3 was used to fit a continuous correlation model. Using the Fisher transformation to stabilize the variance of the correlations and the functional form proposed by Baker and Jayaram (2008), the continuous model for correlations between $Sa(T_1)$ and $Sa(T_2)$ residuals is

$$\rho_{Sa_1,Sa_2}\begin{cases} C_1 & if \quad T_{\min} > 0.06 \\ C_2 & if \quad T_{\max} < 0.06 \\ \min(C_2, C_3) & if \quad T_{\max} < 0.2 \\ C_3 & if \quad T_{max} \geq 0.2 \end{cases} \tag{8}$$

where $T_{\min} = \min(T_1, T_2)$ and $T_{\max} = \max(T_1, T_2)$, and the coefficients C_1, C_2, and C_3 are

$$C_1 = 1 - \cos\left(\frac{\pi}{2} - 0.268 \ln \frac{T_{\max}}{\max(T_{\min}, 0.075)}\right) \tag{9a}$$

$$C_2 = \begin{cases} 1 - 0.12\left(1 - \frac{1}{1+\exp(100T_{\max}-5)}\right)\left(\frac{T_{\max}-T_{\min}}{T_{\max}-0.0099}\right) & if \quad T_{\max} < 0.2 \\ 0 & if \quad T_{\max} \geq 0.2 \end{cases} \tag{9b}$$

$$C_3 = C_1 + 0.267\left(\sqrt{C_4} - C_4\right)\left(1 + \cos\left(\frac{\pi T_{\min}}{0.075}\right)\right) \tag{9c}$$

where

$$C_4 = \begin{cases} C_1 & T_{\max} \geq 0.06 \\ C_2 & T_{\max} < 0.06 \end{cases} \tag{10}$$

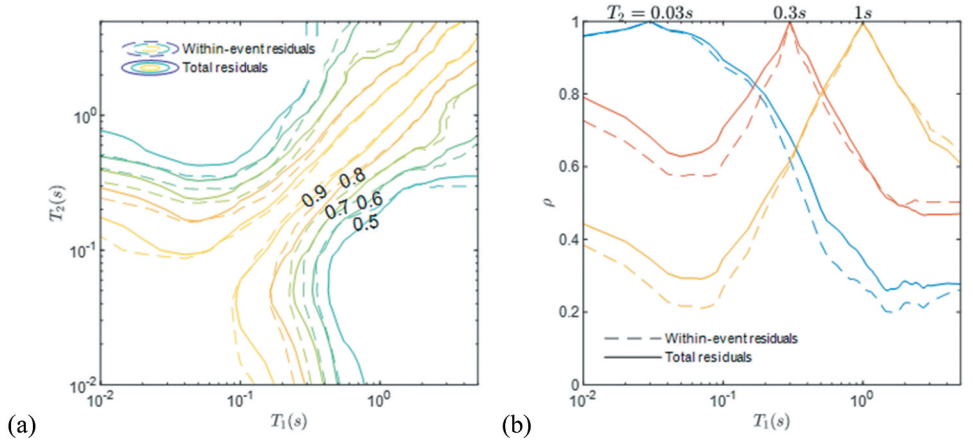

Figure 5. Estimated total residuals (continuous line) and within-event residuals (dashed line) correlation coefficients: (a) Contour plots for periods T_1 and T_2 between 0.01 s and 5 s and (b) for periods T_2=0.03 s, 0.3 s , and 1 s.

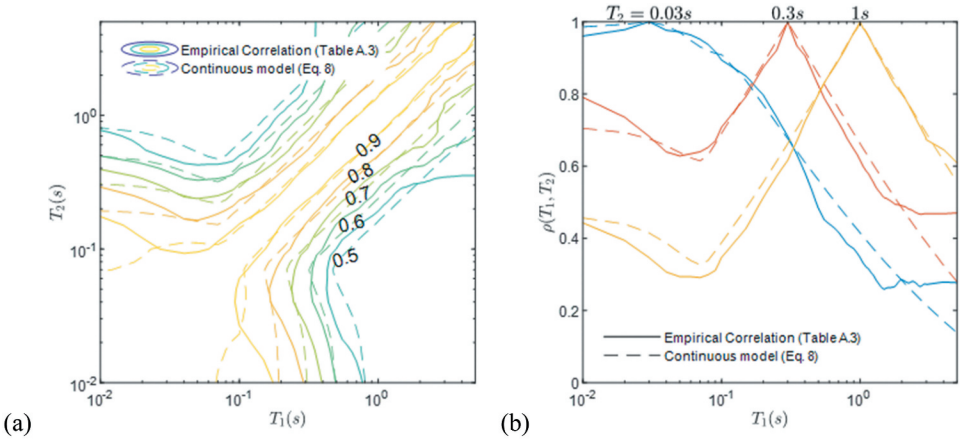

Figure 6. Comparison between the estimated (continuous line) and the predicted (dashed line) correlation coefficients: (a) Contour plots for periods T_1 and T_2 between 0.01 s and 5 s and (b) for periods T_2=0.03 s, 0.3 s, and 1 s.

In addition, *Sa* correlations between *PGA* and *PGV* were computed. The results are summarized in Table A3, Table A4, and Table A5. From the results, it is apparent that $\rho_{PGA,Sa(T)}$ values are almost identical to $\rho_{Sa(T=0.01s),Sa(T)}$ for the period range analyzed. Thus, $\rho_{PGA,Sa(T)}$ can be approximated using Equation 8 under the mild assumption $PGA \approx Sa(T = 0.01s)$. A predictive model was developed for $\rho_{PGV,Sa(T)}$, by means of the total residuals of *PGV* and different *Sa* ordinates. The resulting expression has the form

$$\rho_{PGV,Sa(T)} = \tanh(a_0 + a_1 \cos(a_3 p) - a_2 \sin(a_3 p)\ ) \tag{11}$$

where $\tanh(\Delta)$ is the hyperbolic tangent function and $p = \log_{10} T$. Table A6 summarizes the coefficients a_0 to a_3.

The proposed continuous model for *Sa* correlations at two different periods T_1 and T_2 is in good agreement with the empirical values, with errors not exceeding 11%. Figure 6 shows the contour plot of both the empirical and predicted correlation coefficients. Although the functional form of the correlation model proposed by Baker and Jayaram (2008) was adopted for simplicity, different functional forms can be used.

3. Discussion and Application of the Results

3.1. Comparison with Worldwide Studies

As discussed previously, many studies have focused their attention on estimating inter-period correlations of ground motions in shallow-crustal regions. However, only a few of them address the problem of correlations within subduction zones. The current study accounts for correlations between PGA, PGV, and Sa using specific GMPEs for Mexican intraslab earthquakes. Other ground-motion IMs could be considered in future studies as their GMPEs become available. In the following, the correlation model developed in this study for Sa pairs is compared to those proposed by Baker and Jayaram (2008), Jayaram et al. (2011), Abrahamson, Gregor, and Addo (2016), and Jaimes and Candia (2019). The comparisons are presented in Figs. 7 and 8 in terms of $\rho(T_1, T_2)$ versus T_1, with 0.01 s $\leq T_1 \leq$ 5 s and T_2=0.05 s, 0.1 s, 0.2 s, 0.5 s, 2 s, and 5 s. A shaded region was added around the mean values obtained from Equation 8 and Equation 9 depicting the mean ± one standard deviation. The latter is defined as $SE\left(\rho_{Sa1,Sa2}\right) = \left(1 - \rho_{Sa1,Sa2}{}^2\right)(n-1)^{-0.5}$, where n is the number of ground motions in the dataset (Kotha, Bindi, and Cotton 2017).

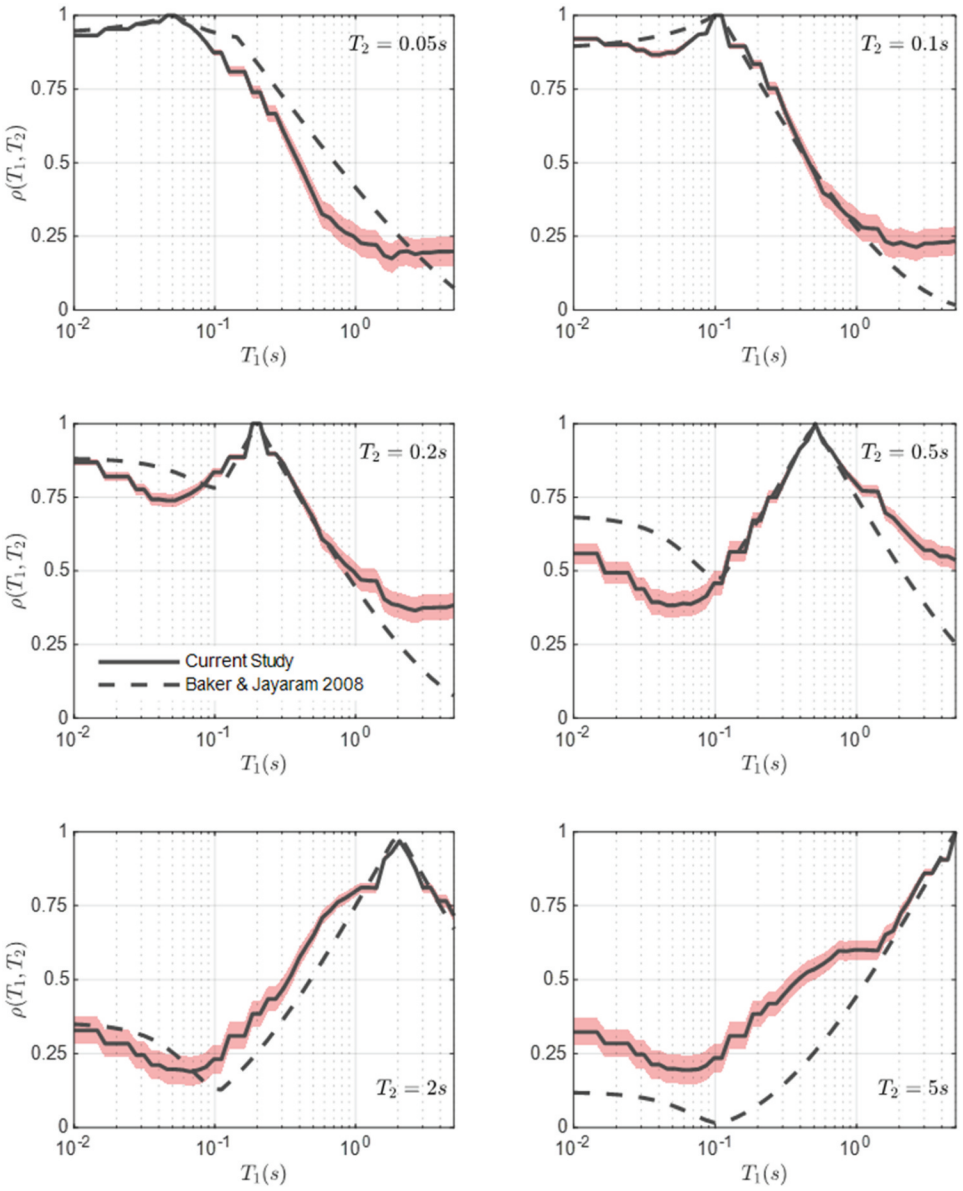

Figure 7. Comparison between correlation models for shallow-crustal earthquakes (Baker and Jayaram 2008) and intermediate-depth, intraslab earthquakes (current study).

In Fig. 7 a reasonable agreement between the correlation model by Baker and Jayaram (2008) for shallow-crustal regions and the model herein is observed. Differences up to ~0.30 units are noticed particularly when one of the periods is close to 5 s. Similar trends have been reported for other tectonic environments (e.g., Candia et al. 2020).

Figure 8 compares the correlation model for Mexican intermediate-depth (intraslab) earthquakes developed in the current study with those by Jayaram et al. (2011) for Japan, Abrahamson, Gregor, and Addo (2016), who used a global dataset but largely dominated by earthquakes from Japan and Taiwan, and Jaimes and Candia (2019) for Mexican interface earthquakes. These plots suggest that the underlying ground motion database and tectonic setting may have a considerable impact on the correlation values; these differences accentuate as T_1 and T_2 depart from each other.

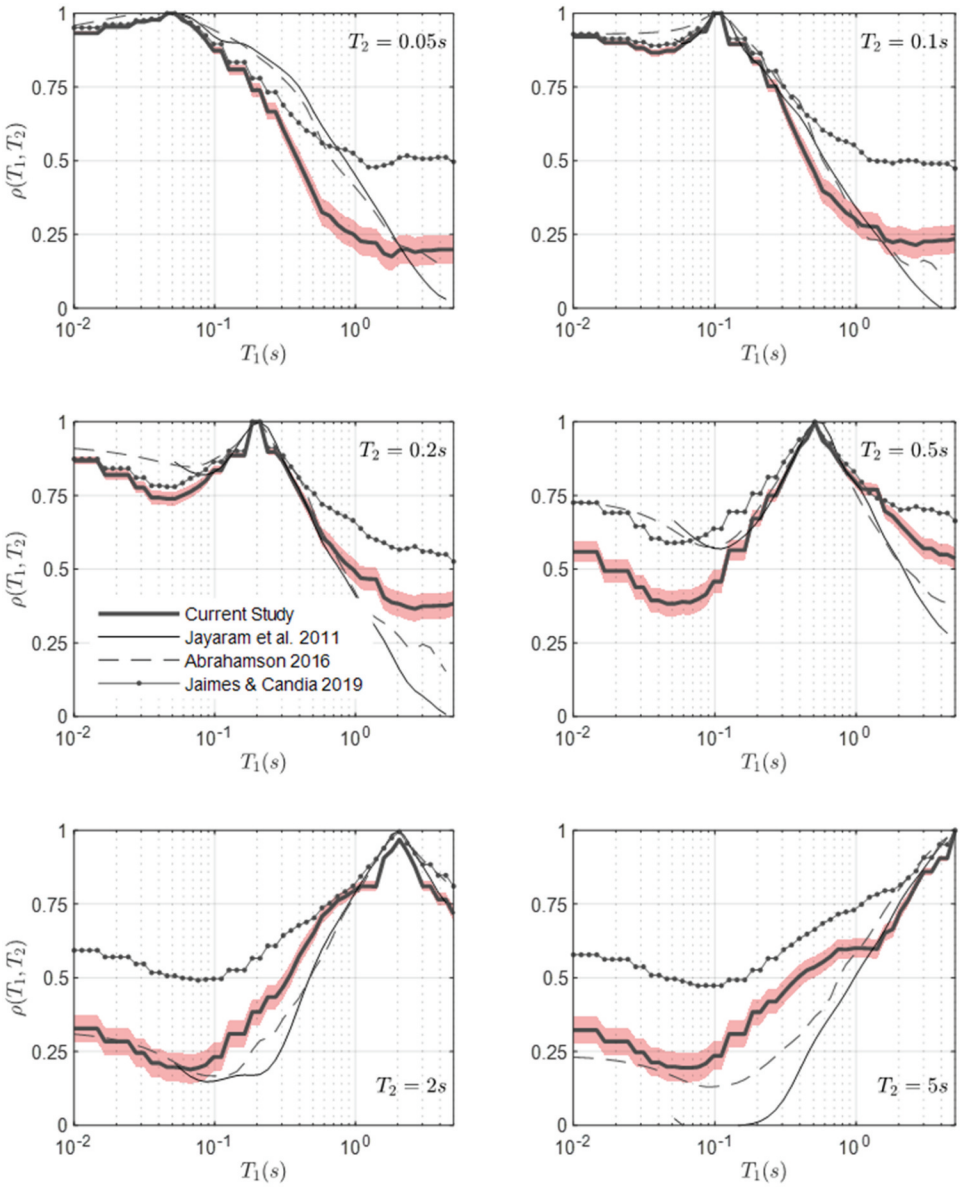

Figure 8. Comparison between correlation models from Mexican intermediate-depth, intraslab earthquakes (current study) and from interface earthquakes: Japan (Jayaram et al. 2011), Global Data (Abrahamson, Gregor, and Addo 2016), and Mexico (Jaimes and Candia 2019).

The differences shown in Figs. 7 and 8 persist after normalizing the periods by $T_{amp1.5}$ – the shortest period at which the response spectral value for each ground motion is 1.5 times the PGA – as suggested by Carlton and Abrahamson (2014). In addition to the tectonic regime, these differences might be attributed to local site conditions. It should be noted that the current study includes only NEHRP class B sites, while Baker and Jayaram (2008) used heterogeneous site classes. In this regard, the direct application of the correlation coefficients reported in this work may not be appropriate to estimate ground-motion correlations on site conditions other than rock or firm soil.

3.2. Application: Conditional Mean Spectrum

The current results are useful in engineering practice as the knowledge of ground-motion correlations has gained popularity in modern seismic hazard calculations and in the generation of design ground motions. To illustrate the applicability of the proposed correlation model, a CMS associated to a uniform hazard spectrum (UHS) with return period of 250 years is analysed for a site located in south-central Mexico, a region controlled by subduction slab seismicity. The site is located near the recording station RABO (18.5691°N, 98.4454°W), which is only 5 km west from the epicentrer of the September 19, 2017 earthquake (M_w=7.1). The seismic hazard for a conditioning period $T^* = 1$ s was obtained using the source geometry and magnitude recurrence model described in Jaimes and Candia (2019).

As shown in Fig. 9(a), the hazard at the site of interest and the design level considered is largely controlled by intraslab seismicity. The mean magnitude and distance of the $Sa(T^* = 1\text{s})$ hazard deaggregation resulted in $\bar{M}$=7.43 and $\bar{R}$=119 km, respectively –see Fig. 9(b)–. For this scenario, the mean response spectrum, as per Jaimes and García-Soto (2020), and the UHS for a 250 year return period are plotted in Fig. 9(c). The resulting CMS as well as CMS ± one standard deviation curves are presented in Fig. 9(d); they were obtained using the following equations (Baker 2011):

$$\ln(Sa(T_i|T^*)) = \overline{\ln(Sa(T_i))} + \varepsilon(T^*) \cdot \rho_{T_i,T^*} \cdot \sigma(T_i) \tag{12a}$$

$$\sigma_{\ln(Sa(T_i))|\ln(Sa(T^*))} = \sigma(T_i)\sqrt{1 - \rho^2_{T_i,T^*}} \tag{12b}$$

where $\overline{\ln(Sa(T_i))}$ and $\sigma(T_i)$ are the mean and standard deviation obtained from the GMPE; ρ_{T_i,T^*} is the correlation between T^* and other periods T_i as in Equation 8; and $\varepsilon(T^*)$ is the number of standard deviations between $\overline{\ln(Sa(T^*))}$ and UHS (T^*) at the conditioning period T^*=1 s, that is

$$\varepsilon(T^*) = \frac{\overline{\ln(Sa(T^*))} - \text{UHS}(T^*)}{\sigma(T^*)} \tag{13}$$

A similar procedure was applied for conditioning periods T^* equal to 0.5 s and 2 s. The resulting CMS as well as CMS ± one standard deviation curves are presented in Figs. A1 and A2. Note that Mexican regulations for seismic design as MOC (CFE 2016) require that the spectral ordinates of the ground motions used in dynamic analyses be bounded by the mean ± one standard deviation, within the period range given by the shaded area shown in Figs. A1 and A2.

The influence of three different correlation models in the CMS was also analysed in this study. The results indicate that using different models does not affect the hazard at the site of interest. Here, Fig. 10 shows the CMSs computed using the correction coefficients proposed by Baker and Jayaram (2008), Jaimes and Candia (2019), and the current study. Differences up to 20% are observed between the CMSs for periods below 0.5 s. Similar results were found when considering T^*=0.5 s or 2 s (see Figs. A3 and A4).

4. Conclusions

This paper presents empirical correlation coefficients between peak ground acceleration, peak ground velocity, and spectral accelerations from Mexican intermediate-depth, intraslab earthquakes, as well as a simplified prediction model to approximate these values. The correlations were obtained using GMPEs proposed by Jaimes and García-Soto (2020) and the RAII-UNAM strong-motion database. The results were compared with those reported in worldwide studies, which include correlation models from both interface earthquakes (Abrahamson, Gregor, and Addo 2016; Jaimes and Candia 2019; Jayaram et al. 2011) and shallow-crustal earthquakes (Baker and Jayaram 2008). The results show large statistical differences between the correlation model for intraslab Mexican earthquakes, shallow-crustal earthquakes, and subduction earthquakes from elsewhere. We cannot (yet) relate these

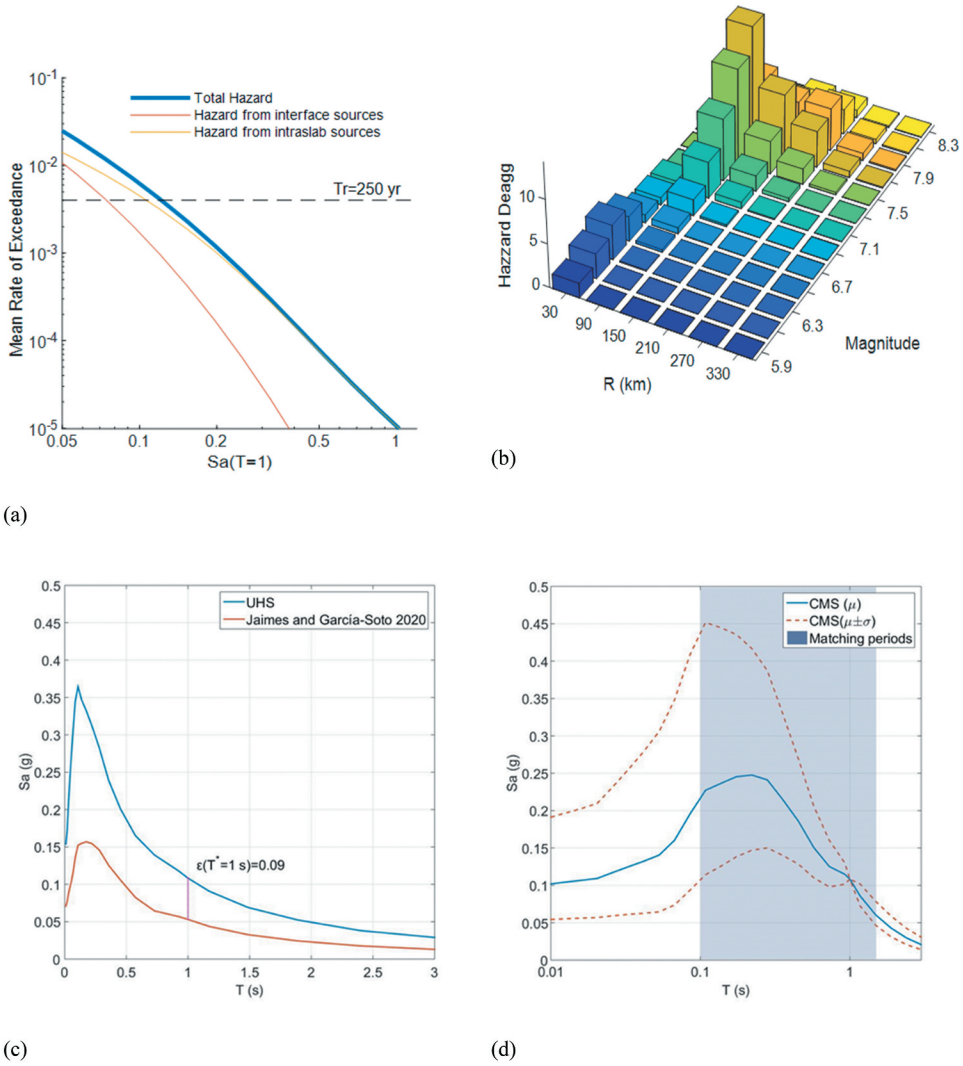

Figure 9. (a) Hazard curve for T^*=1 s at a site near station RABO; (b) $Sa(T^* = 1s)$ hazard deaggregation for a return period of 250 years; (c) mean response spectrum computed using Equation 7 (Jaimes and García-Soto 2020) and USH for a return period of 250 year; and (d) CMS at the site RABO.

results to the physical parameters of earthquakes, and more research is required to explain these differences, as well as their effect on the ground-motion characterization. Meanwhile, we recommend the use of a region- and mechanism-specific correlation models for southcentral Mexico, an area with seismicity controlled by subduction earthquakes. Similar observations regarding the applicability of global versus regional model can be found in other studies (Candia et al. 2020; Jayaram et al. 2011).

The correlation models presented in this paper provide key information for a variety of earthquake engineering applications where the joint occurrence of multiple ground-motion IMs is needed. In this regard, an illustrative example of a CMS is given, in which the knowledge of the correlation structure allows to significantly reduce the pseudo-acceleration ordinates compared to a UHS.

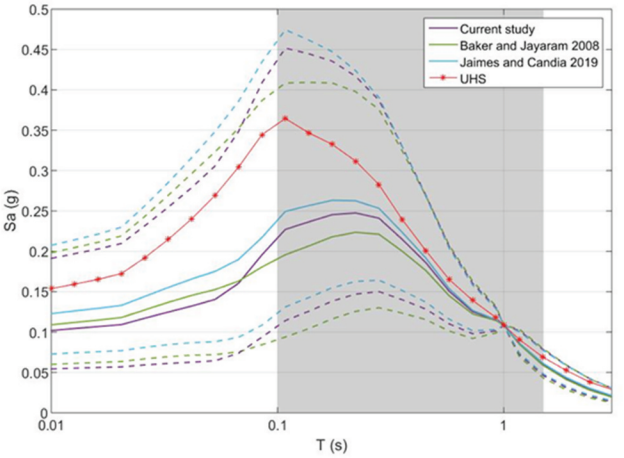

Figure 10. CMSs computed using different correlation coefficient models for T^*=1 s.

Acknowledgments

The studies by García et al. (2005) and García (2006), as well as those by Hong, García-Soto, and Gómez (2010), Arroyo et al. (2010), and García-Soto, Hong, and Gómez (2012), and a recent study by Jaimes and García-Soto (2020), are part of the references from which the ground-motion data were selected. Also, strong-motion data from 2005 to 2019 were obtained from the catalogues provided by UNAM Institute of Engineering (II-UNAM 2020) and UNAM Institute of Geophysics (Geofísica-UNAM 2020). This research was financially supported by Instituto de Ingeniería at UNAM through the Research Fund R528. Additional support was sponsored by the Proyect IN102021 "Estudio de riesgo sísmico de edificios existentes denominados de planta baja débil con un sistema rotacional". Dr. Candia received financial support from ANID/FONDECYT Grant 11180937 "Seismic Risk of Mined Tunnels" and the National Research Center for Integrated Natural Disaster Management (CIGIDEN) ANID/FONDAP/15110017, and Facultad de Ingeniería Civil at Universidad del Desarrollo.

Disclosure Statement

No potential conflict of interest was reported by the author(s).

ORCID

Alhelí S. López-Castañeda http://orcid.org/0000-0001-9449-2568

References

Abrahamson, N. A., N. Gregor, and K. Addo. 2016. BC hydro ground motion prediction equations for subduction earthquakes. *Earthquake Spectra* 32 (1): 23–44. doi: 10.1193/051712EQS188MR.

Arroyo, D., D. García, M. Ordaz, M. A. Mora, and S. K. Singh. 2010. Strong ground-motion relations for Mexican interplate earthquakes. *Journal of Seismology* 14 (4): 769–85. doi: 10.1007/s10950-010-9200-0.

Azarbakht, A., M. Mousavi, M. Nourizadeh, and M. Shahri. 2014. Dependence of correlations between spectral accelerations at multiple periods on magnitude and distance. *Earthquake Engineering & Structural Dynamics* 43 (8): 1193–204. doi: 10.1002/eqe.2393.

Baker, J. W., and C. A. Cornell. 2006. Correlation of response spectral values for multicomponent ground motions. *Bulletin of the Seismological Society of America* 96 (1): 215–27. doi: 10.1785/0120050060.

Baker, J. W., and N. Jayaram. 2008. Correlation of spectral acceleration values from NGA ground motion models. *Earthquake Spectra* 24 (1): 299–317. doi: 10.1193/1.2857544.

Baker, J. W. 2011. Conditional mean spectrum: Tool for ground-motion selection. *Journal of Structural Engineering* 137 (3): 322–31. doi: 10.1061/(ASCE)ST.1943-541X.0000215.

Bazzurro, P., and C. A. Cornell. 2002. Vector-valued probabilistic seismic hazard analysis (VPHSA). In *7th U.S. National Conference on Earthquake Engineering*. Boston, Massachusetts.

Bindi, D., M. Massa, G. Luzi, F. Pacor, R. Puglia, and P. Augliera. 2014. Pan-European ground-motion prediction equations for the average horizontal component of PGA, PGV, and 5 %-damped PSA at spectral periods up to 3.0 s using the RESOURCE dataset. *Bulletin of Earthquake Engineering* 12 (1): 391–430. doi: 10.1007/s10518-013-9525-5.

Bradley, B. A. 2011. Correlation of significant duration with amplitude and cumulative intensity measures and its use in ground motion selection. *Journal of Earthquake Engineering* 15 (6): 809–32. doi: 10.1080/13632469.2011.557140.

Candia, G., A. Poulos, J. C. de La Llera, J. G. F. Crempien, and J. Macedo. 2020. Correlations of spectral accelerations in the Chilean subduction zone. *Earthquake Spectra* 36 (2): 788–805. doi: 10.1177/8755293019891723.

Carlton, B., and N. A. Abrahamson. 2014. Issues and approaches for implementing conditional mean spectra in practice. *Bulletin of the Seismological Society of America* 104 (1): 203–512. doi: 10.1785/0120130129.

Chiou, B., R. Darragh, N. Gregor, and W. Silva. 2008. NGA project strong-motion database. *Earthquake Spectra* 24 (1): 23–44. doi: 10.1193/1.2894831.

Comisión Federal de Electricidad (CFE). 2016. *Manual de Obras Civiles: Diseño por Sismo*.

Cordova, P. P., G. G. Deierlein, S. S. F. Mehanny, and C. A. Cornell. 2001. Development of a two-parameter seismic intensity measure and probabilistic assessment procedure. In *The second US-Japan workshop on performance-based earthquake engineering methodology for reinforced concrete building structures*, 187–206. Hokkaido, Japan.

Daneshvar, P., N. Bouaanani, and A. Godia. 2015. On computation of conditional mean spectrum in Eastern Canada. *Journal of Seismology* 19 (1): 443–67. doi: 10.1007/s10950-014-9476-6.

García-Soto, A. D., H. P. Hong, and R. Gómez. 2012. Effect of the orientation of records on displacement ductility demand. *Canadian Journal of Civil Engineering* 39 (4): 362–73. doi: 10.1139/l2012-010.

García, D., S. K. Singh, M. Herráiz, M. Ordaz, and J. F. Pacheco. 2005. Inslab earthquakes of Central Mexico: Peak ground-motion parameters and response spectra. *Bulletin of the Seismological Society of America* 95 (6): 2272–82. doi: 10.1785/0120050072.

García, D. 2006. *Estimación de parámetros del movimiento fuerte del suelo para terremotos interplaca e intraslab en México central*. Madrid: Facultad de Ciencias Físicas, Universidad Complutense de Madrid.

Goda, K., and G. M. Atkinson. 2009. Probabilistic characterization of spatially correlated response spectra for earthqaukes in Japan. *Bulletin of the Seismological Society of America* 99 (5): 3003–20. doi: 10.1785/0120090007.

Hong, H. P., A. D. García-Soto, and R. Gómez. 2010. Impact of different earthquake types on the statistics of ductility of demand. *Journal of Structural Engineering* 136 (7): 770–80. doi: 10.1061/_ASCE_ST.1943-541X.0000177.

Inoue, T., and C. A. Cornell. 1990. *Seismic hazard analysis of multi-degree-of-freedom structures, reliability of marine structures*. Stanford, California: Stanford University.

Instituto de Geofísica de la Universidad Nacional Autónoma de México (Geofísica-UNAM). 2020. Servicio Sismológico Nacional.

Instituto de Ingeniería de la Univerisdad Nacional Autónoma de México (II-UNAM). 2020. Red acelerográfica del Instituto de Ingeniería (RAII-UNAM).

Jaimes, M. A., and A. D. García-Soto. 2020. Updated ground motion prediction model for Mexican intermediate-depth intraslab earthquakes including V/H ratios. *Earthquake Spectra* 36 (3): 1298–330. doi: 10.1177/8755293019899947.

Jaimes, M. A., and G. Candia. 2019. Interperiod correlation model for Mexican interface earthquakes. *Earthquake Spectra* 35 (3): 1351–65. doi: 10.1193/080918EQS200M.

Jayaram, N., J. W. Baker, H. Okano, H. Ishida, M. W. McCann Jr., and Y. Mihara. 2011. Correlation of response spectral values in Japanese ground motions. *Earthquakes and Structures* 2 (4): 357–76. doi: 10.12989/eas.2011.2.4.357.

Kotha, S. R., D. Bindi, and F. Cotton. 2017. Site-corrected magnitude- and region-dependent correlations of horizontal peak spectral amplitudes. *Earthquake Spectra* 33 (4): 1415–32. doi: 10.1193/091416eqs150m.

Lin, T., S. C. Harmsen, J. W. Baker, and N. Luco. 2013. Conditional spectrum computation incorporating multiple causal earthquakes and ground-motion prediction models. *Bulletin of the Seismological Society of America* 103 (2A): 1103–16. doi: 10.1785/0120110293.

Trombetti, T., S. Silvestri, G. Gasparini, M. Righi, and C. Ceccoli. 2008. Correlations between the displacement response spectra and the parameters characterising the magnitude of the ground motion. In *Proceedings of the 14th World Conference on Earthquake Engineering*. Bejing.

Appendix

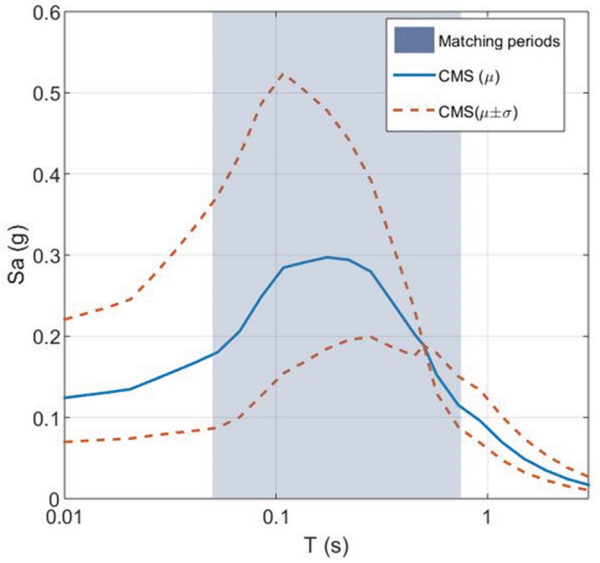

Figure A1. CMS and CMS ± one standard deviation curves computed considering T^*=0.5 s.

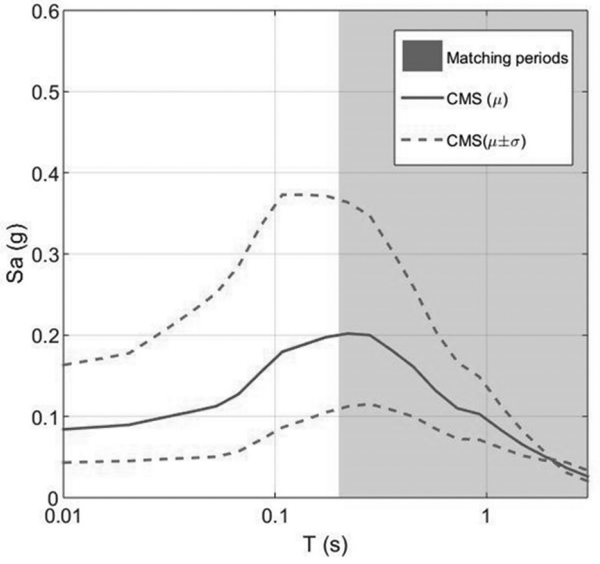

Figure A2. CMS and CMS ± one standard deviation curves computed considering T^*=2 s.

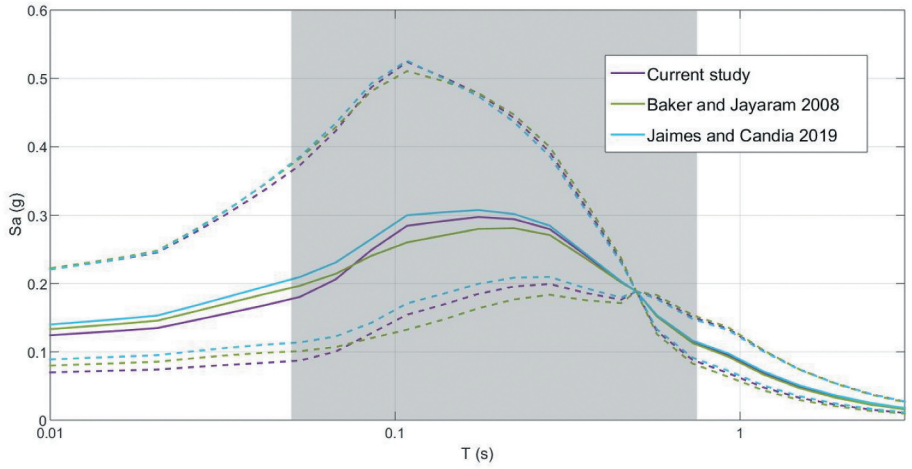

Figure A3. CMSs computed using different correlation coefficient models for T^*=0.5 s, continuous lines stand the mean CMS and dashed lines stand for the mean CMS ± one standard deviation.

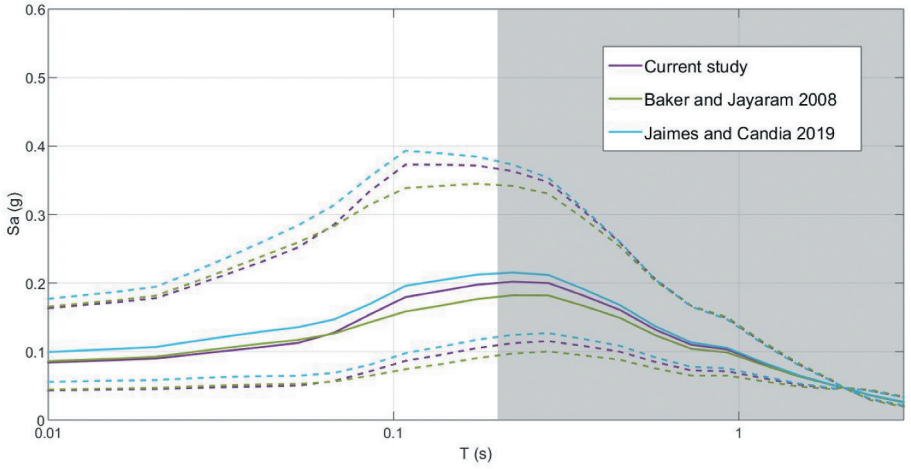

Figure A4. CMSs computed using different correlation coefficient models for T^*=2 s, continuous lines stand for the mean CMS and dashed lines stand for the mean CMS ± one standard deviation.

Table A1. Summary of events used in the analysis.

Event	Date (yy/mm/dd)	Magnitude, M_w	Focus Location			Number of Recordings
			Lat (°)	Lon (°)	Depth, H_D (km)	
1	94/02/23	5.8	17.75	−97.27	75	6
2	94/05/23	6.2	18.02	−100.57	50	21
3	94/12/10	6.4	17.98	−101.52	50	16
4	97/01/11	7.1	18.34	−102.58	40	22
5	97/05/22	6.5	18.37	−101.82	54	18
6	98/04/20	5.9	18.35	−101.19	64	15
7	99/06/15	6.9	18.13	−97.54	61	30
8	99/06/21	6.3	18.15	−101.70	53	16
9	99/09/30	7.4	16.03	−96.96	47	26
10	99/12/29	5.9	18.00	−101.63	50	14
11	00/07/21	5.9	18.11	−98.97	50	21
12	01/03/05	5.3	17.15	−100.11	35	21
13	01/03/06	5.2	17.14	−100.11	38	23
14	02/01/30	5.9	18.15	−95.98	118	13
15	04/01/17	5.4	17.66	−95.66	110	9
16	04/04/20	5.6	17.34	−94.75	138	6
17	09/05/22	5.6	18.22	−98.26	45	10
18	11/12/11	6.5	17.89	−99.84	58	21
19	13/06/16	5.8	18.25	−99.18	60	13
20	14/07/29	6.4	17.97	−95.69	117	11
21	15/03/20	5.4	18.12	−98.35	61	7
22	17/09/08	8.2	14.85	−94.11	58	9
23	17/09/19	7.1	18.40	−98.72	57	18

Table A2. Regression parameters a and σ for *Sa* GMPE (Jaimes and García-Soto 2020).

T(s)	a_1	a_2	a_3	a_4	a_5	σ_B	σ_W	σ
0.01	0.1824	1.3569	−1.0	−0.0084	0.0266	0.36	0.60	0.70
0.02	0.3380	1.3502	−1.0	−0.0086	0.0262	0.37	0.61	0.71
0.06	1.2826	1.2732	−1.0	−0.0088	0.0263	0.47	0.69	0.83
0.08	1.5138	1.2680	−1.0	−0.0088	0.0272	0.42	0.69	0.81
0.1	1.5392	1.2800	−1.0	−0.0085	0.0284	0.34	0.70	0.78
0.2	0.4035	1.4283	−1.0	−0.0081	0.0284	0.34	0.57	0.67
0.3	−0.7722	1.5597	−1.0	−0.0075	0.0231	0.34	0.53	0.63
0.4	−1.4572	1.5975	−1.0	−0.0063	0.0216	0.30	0.54	0.62
0.5	−2.0213	1.6378	−1.0	−0.0055	0.0153	0.24	0.54	0.59
0.6	−2.3061	1.6297	−1.0	−0.0048	0.0178	0.21	0.56	0.60
0.7	−2.5725	1.6332	−1.0	−0.0043	0.0165	0.20	0.58	0.61
0.8	−3.0802	1.6927	−1.0	−0.0043	0.0137	0.21	0.57	0.61
0.9	−3.5864	1.7458	−1.0	−0.0040	0.0134	0.21	0.57	0.61
1	−3.9575	1.7752	−1.0	−0.0036	0.0123	0.19	0.57	0.61
2	−6.2968	1.9592	−1.0	−0.0029	0.0072	0.18	0.54	0.57
3	−7.5722	2.0386	−1.0	−0.0021	0.0044	0.26	0.49	0.55
4	−8.7329	2.1320	−1.0	−0.0017	0.0046	0.22	0.49	0.53
5	−9.6803	2.2118	−1.0	−0.0016	0.0041	0.19	0.48	0.51
PGA	0.1571	1.3581	−1.0	−0.0084	0.0268	0.35	0.60	0.70
PGV	−5.0446	1.6401	−1.0	−0.0054	0.0135	0.25	0.54	0.60

Table A3. Total correlation coefficients.

$T(s)$	**0.01**	**0.02**	**0.06**	**0.08**	**0.1**	**0.2**	**0.3**	**0.5**	**0.7**	**0.8**	**0.9**	**1**	**2**	**3**	**4**	**5**	**PGA**	**PGV**
0.01	1.000	0.983	0.936	0.934	0.926	0.876	0.767	0.550	0.472	0.431	0.421	0.403	0.332	0.314	0.306	0.305	0.999	0.737
0.02	0.983	1.000	0.951	0.933	0.908	0.826	0.707	0.483	0.416	0.374	0.369	0.349	0.288	0.272	0.265	0.267	0.979	0.682
0.06	0.936	0.951	1.000	0.958	0.906	0.751	0.611	0.384	0.308	0.270	0.267	0.247	0.203	0.198	0.183	0.173	0.931	0.579
0.08	0.934	0.933	0.958	1.000	0.957	0.777	0.625	0.389	0.317	0.279	0.273	0.244	0.201	0.198	0.181	0.177	0.931	0.584
0.1	0.926	0.908	0.906	0.957	1.000	0.806	0.644	0.412	0.336	0.291	0.286	0.265	0.206	0.198	0.189	0.188	0.927	0.588
0.2	0.876	0.826	0.751	0.777	0.806	1.000	0.869	0.692	0.597	0.557	0.539	0.514	0.408	0.402	0.386	0.392	0.881	0.776
0.3	0.767	0.707	0.611	0.625	0.644	0.869	1.000	0.803	0.679	0.626	0.604	0.579	0.453	0.445	0.424	0.438	0.774	0.813
0.5	0.550	0.483	0.384	0.389	0.412	0.692	0.803	1.000	0.894	0.855	0.818	0.791	0.653	0.581	0.543	0.537	0.559	0.842
0.7	0.472	0.416	0.308	0.317	0.336	0.597	0.679	0.894	1.000	0.959	0.921	0.888	0.748	0.666	0.631	0.588	0.480	0.821
0.8	0.431	0.374	0.270	0.279	0.291	0.557	0.626	0.855	0.959	1.000	0.964	0.927	0.764	0.662	0.631	0.597	0.439	0.804
0.9	0.421	0.369	0.267	0.273	0.286	0.539	0.604	0.818	0.921	0.964	1.000	0.969	0.774	0.656	0.623	0.593	0.429	0.795
1	0.403	0.349	0.247	0.244	0.265	0.514	0.579	0.791	0.888	0.927	0.969	1.000	0.792	0.672	0.643	0.603	0.412	0.788
2	0.332	0.288	0.203	0.201	0.206	0.408	0.453	0.653	0.748	0.764	0.774	0.792	1.000	0.839	0.782	0.728	0.339	0.737
3	0.314	0.272	0.198	0.198	0.198	0.402	0.445	0.581	0.666	0.662	0.656	0.672	0.839	1.000	0.913	0.831	0.321	0.696
4	0.306	0.265	0.183	0.181	0.189	0.386	0.424	0.543	0.631	0.631	0.623	0.643	0.782	0.913	1.000	0.934	0.312	0.674
5	0.305	0.267	0.173	0.177	0.188	0.392	0.438	0.537	0.588	0.597	0.593	0.603	0.728	0.831	0.934	1.000	0.311	0.659
PGA	0.999	0.979	0.931	0.931	0.927	0.881	0.774	0.559	0.480	0.439	0.429	0.412	0.339	0.321	0.312	0.311	1.000	0.744
PGV	0.737	0.682	0.579	0.584	0.588	0.776	0.813	0.842	0.821	0.804	0.795	0.788	0.737	0.696	0.674	0.659	0.744	1.000

Table A4. Between-events correlation coefficients.

T(s)	0.01	0.02	0.06	0.08	0.1	0.2	0.3	0.5	0.7	0.8	0.9	1	2	3	4	5	PGA	PGV
0.01	1.000	0.981	0.941	0.926	0.915	0.865	0.731	0.512	0.442	0.411	0.416	0.403	0.334	0.327	0.337	0.336	0.999	0.701
0.02	0.981	1.000	0.949	0.920	0.896	0.817	0.671	0.442	0.382	0.348	0.358	0.343	0.283	0.277	0.290	0.296	0.976	0.638
0.06	0.941	0.949	1.000	0.950	0.915	0.760	0.582	0.344	0.265	0.235	0.247	0.232	0.183	0.176	0.185	0.182	0.936	0.528
0.08	0.926	0.920	0.950	1.000	0.962	0.767	0.580	0.337	0.268	0.239	0.248	0.223	0.179	0.170	0.174	0.175	0.924	0.524
0.1	0.915	0.896	0.915	0.962	1.000	0.775	0.586	0.356	0.285	0.250	0.260	0.245	0.188	0.175	0.183	0.182	0.915	0.531
0.2	0.865	0.817	0.760	0.767	0.775	1.000	0.838	0.666	0.584	0.556	0.556	0.537	0.434	0.437	0.428	0.425	0.868	0.759
0.3	0.731	0.671	0.582	0.580	0.586	0.838	1.000	0.793	0.682	0.633	0.626	0.608	0.488	0.508	0.497	0.505	0.738	0.807
0.5	0.512	0.442	0.344	0.337	0.356	0.666	0.793	1.000	0.893	0.852	0.818	0.794	0.670	0.629	0.589	0.578	0.521	0.837
0.7	0.442	0.382	0.265	0.268	0.285	0.584	0.682	0.893	1.000	0.958	0.920	0.887	0.759	0.703	0.663	0.616	0.451	0.820
0.8	0.411	0.348	0.235	0.239	0.250	0.556	0.633	0.852	0.958	1.000	0.961	0.922	0.776	0.706	0.667	0.631	0.420	0.809
0.9	0.416	0.358	0.247	0.248	0.260	0.556	0.626	0.818	0.920	0.961	1.000	0.967	0.785	0.703	0.662	0.631	0.425	0.808
1	0.403	0.343	0.232	0.223	0.245	0.537	0.608	0.794	0.887	0.922	0.967	1.000	0.799	0.714	0.678	0.636	0.413	0.803
2	0.334	0.283	0.183	0.179	0.188	0.434	0.488	0.670	0.759	0.776	0.785	0.799	1.000	0.845	0.786	0.732	0.343	0.757
3	0.327	0.277	0.176	0.170	0.175	0.437	0.508	0.629	0.703	0.706	0.703	0.714	0.845	1.000	0.909	0.824	0.336	0.746
4	0.337	0.290	0.185	0.174	0.183	0.428	0.497	0.589	0.663	0.667	0.662	0.678	0.786	0.909	1.000	0.927	0.344	0.729
5	0.336	0.296	0.182	0.175	0.182	0.425	0.505	0.578	0.616	0.631	0.631	0.636	0.732	0.824	0.927	1.000	0.342	0.711
PGA	0.999	0.976	0.936	0.924	0.915	0.868	0.738	0.521	0.451	0.420	0.425	0.413	0.343	0.336	0.344	0.342	1.000	0.709
PGV	0.701	0.638	0.528	0.524	0.531	0.759	0.807	0.837	0.820	0.809	0.808	0.803	0.757	0.746	0.729	0.711	0.709	1.000

Table A5. Within-event correlation coefficients.

$T(s)$	**0.01**	**0.02**	**0.06**	**0.08**	**0.1**	**0.2**	**0.3**	**0.5**	**0.7**	**0.8**	**0.9**	**1**	**2**	**3**	**4**	**5**	**PGA**	**PGV**
0.01	1.000	0.991	0.924	0.962	0.981	0.916	0.880	0.736	0.675	0.562	0.478	0.440	0.362	0.267	0.174	0.170	1.000	0.915
0.02	0.991	1.000	0.961	0.982	0.961	0.859	0.824	0.683	0.639	0.532	0.453	0.416	0.353	0.253	0.157	0.139	0.988	0.894
0.06	0.924	0.961	1.000	0.988	0.891	0.726	0.696	0.570	0.561	0.461	0.394	0.354	0.347	0.275	0.183	0.139	0.916	0.811
0.08	0.962	0.982	0.988	1.000	0.944	0.813	0.768	0.633	0.617	0.506	0.428	0.385	0.363	0.302	0.220	0.194	0.957	0.860
0.1	0.981	0.961	0.891	0.944	1.000	0.939	0.872	0.711	0.676	0.545	0.453	0.408	0.342	0.298	0.221	0.227	0.983	0.886
0.2	0.916	0.859	0.726	0.813	0.939	1.000	0.952	0.834	0.739	0.623	0.521	0.477	0.341	0.288	0.240	0.281	0.925	0.882
0.3	0.880	0.824	0.696	0.768	0.872	0.952	1.000	0.899	0.768	0.677	0.585	0.534	0.370	0.252	0.174	0.201	0.886	0.886
0.5	0.736	0.683	0.570	0.633	0.711	0.834	0.899	1.000	0.917	0.889	0.825	0.787	0.543	0.358	0.282	0.283	0.743	0.867
0.7	0.675	0.639	0.561	0.617	0.676	0.739	0.768	0.917	1.000	0.969	0.927	0.894	0.651	0.489	0.425	0.384	0.680	0.846
0.8	0.562	0.532	0.461	0.506	0.545	0.623	0.677	0.889	0.969	1.000	0.987	0.964	0.672	0.447	0.397	0.354	0.567	0.782
0.9	0.478	0.453	0.394	0.428	0.453	0.521	0.585	0.825	0.927	0.987	1.000	0.989	0.681	0.422	0.371	0.316	0.482	0.722
1	0.440	0.416	0.354	0.385	0.408	0.477	0.534	0.787	0.894	0.964	0.989	1.000	0.731	0.466	0.414	0.358	0.445	0.700
2	0.362	0.353	0.347	0.363	0.342	0.341	0.370	0.543	0.651	0.672	0.681	0.731	1.000	0.886	0.784	0.715	0.362	0.614
3	0.267	0.253	0.275	0.302	0.298	0.288	0.252	0.358	0.489	0.447	0.422	0.466	0.886	1.000	0.947	0.889	0.268	0.468
4	0.174	0.157	0.183	0.220	0.221	0.240	0.174	0.282	0.425	0.397	0.371	0.414	0.784	0.947	1.000	0.976	0.177	0.368
5	0.170	0.139	0.139	0.194	0.227	0.281	0.201	0.283	0.384	0.354	0.316	0.358	0.715	0.889	0.976	1.000	0.175	0.344
PGA	1.000	0.988	0.916	0.957	0.983	0.925	0.886	0.743	0.680	0.567	0.482	0.445	0.362	0.268	0.177	0.175	1.000	0.917
PGV	0.915	0.894	0.811	0.860	0.886	0.882	0.886	0.867	0.846	0.782	0.722	0.700	0.614	0.468	0.368	0.344	0.917	1.000

Table A6. Regression coefficients for the $\rho_{PGV,Sa(T)}$ model given in Eq. (11).

Parameter	Value
a_0	0.903
a_1	0.189
a_2	−0.082
a_3	2.726